Check for updates

ADVANCED FUNCTIONAL MATERIALS
www.afm-journal.de

Anti-Swelling, High-Strength, Anisotropic Conductive Hydrogel with Excellent Biocompatibility for Implantable Electronic Tendon

Na Li, Qingyu Yu, Sidi Duan, Yingjie Du, Xiaojiao Shi, Xinyu Li, Tifeng Jiao, Zhihui Qin,* and Ximin He**

As hydrogels rapidly advance for diverse technologies, their practical applications as implantable artificial tendon becomes promising, yet challenging. It requires similar anisotropic fibril structures, matching water content, high mechanical strength, good biocompatibility, and stable performance under physiological conditions. Furthermore, the capabilities of real-time joint motion monitoring and implant condition are extremely important for the precise assessment of rehabilitation processes. However, it is challenging to realize all these properties simultaneously. Herein, this work reports an intelligent implantable artificial tendon based on strong and conductive anisotropic hydrogel, by coupling prestretching-induced ordered structure with drying-enabled strengthening. The fiber structure fixed during drying/rehydration produces a dense and stable network with a hierarchically anisotropic structure. The resulting anisotropic hydrogel presents excellent anti-swelling ability (<3%), high tensile strength (3.71 MPa), and toughness (9.86 MJ m^{-3}) upon hydration, at a tendon-matching water content of 72.5 wt%. The in vitro and in vivo tests demonstrate its excellent biocompatibility with significant protein resistance. With reliable strain sensing, the hydrogel can act as an intelligent artificial tendon to restore and real-time monitor joint motion in an in vitro model. The SD rats with tendon defects display restored motor function after implantation of the hydrogel as tendon substitutes, facilitating malfunction tissue therapeutics and rehabilitation.

1. Introduction

Natural structural tissues in biological systems, such as tendons, skeletal muscles, cartilages, and ligaments, exhibit hierarchically anisotropic microscopic structures that give them superior mechanical performances and specific biological functions.[1,2] For instance, tendons, which play a crucial role in joint motion, are high-strength, anisotropic connective tissues composed of a hierarchy of linearly arranged collagen fiber bundles and possess a high water content of 60–80 wt%.[3,4] However, tendon injuries are common muscle disorders with poor or no effective healing capacity.[5,6] The development of high-strength biomimetic materials could provide a promising treatment option for tendon injuries. Among various materials, hydrogels have emerged as an ideal class of synthetic materials due to their structural and compositional similarities to the native extracellular matrix.[7] However, the strength and toughness of conventional hydrogels are usually low, limiting their applications in load-bearing areas.[8] To be suitable for implantable applications as biomimetic artificial tendons, a hydrogel should have excellent mechanical properties with biomimetic anisotropic structure for essential load-bearing capabilities. Additionally, the hydrogel should demonstrate minimal swelling to ensure the stability of its structure and performance in a physiological environment. Finally, good biocompatibility is essential to minimize adverse immune responses after the implantation.

N. Li, X. Shi, X. Li, T. Jiao, Z. Qin
State Key Laboratory of Metastable Materials Science and Technology
Hebei Key Laboratory of Applied Chemistry
Hebei Key Laboratory of Nanobiotechnology
Hebei Key Laboratory of Heavy Metal Deep-Remediation in Water and Resource Reuse
Yanshan University
Qinhuangdao 066004, China
E-mail: tfjiao@ysu.edu.cn; zhqin@ysu.edu.cn

Q. Yu
Institute of Biomedical Engineering
Chinese Academy of Medical Sciences & Peking Union Medical College
Tianjin 300192, China

S. Duan, Y. Du, X. He
Department of Materials Science and Engineering
University of California
Los Angeles, CA 90095, USA
E-mail: ximinhe@ucla.edu

The ORCID identification number(s) for the author(s) of this article can be found under https://doi.org/10.1002/adfm.202309500

DOI: 10.1002/adfm.202309500

 © 2023 Wiley-VCH GmbH

Recently, significant efforts have been devoted to engineering biomimetic hydrogels with anisotropic structures and greatly improved mechanical properties utilizing several methods including mechanical stretching, directional freeze-casting, and the incorporation of additional fillers.[9–15] For example, the combination of freeze-casting with salting-out was used to generate hierarchical structures, leading to the enhanced mechanics of the hydrogels.[9] Despite certain successes in developing anisotropic hydrogels with high strength and toughness comparable to tendons or ligaments, a notable problem that remains is that these hydrogels tend to swell under physiological conditions owing to the intrinsic hydrophilicity and high osmotic pressure inside the network. The swelling of hydrogels can cause remarkable degradation of their mechanical strength and exert pressure on the adjacent tissues.[16–19] Although a few anisotropic hydrogels with minimal swelling have been prepared, these works primarily focused on mechanical properties while ignoring the importance of biocompatibility, especially non-specific protein adsorption.[20,21] When artificial materials are implanted in biological organisms, nonspecific proteins and other components will adsorb onto the surface of the implantable hydrogels.[22,23] Severe protein adsorption can lead to a number of biological reactions in vivo such as inflammation, immune response, and fibrous capsule formation. Such complications can lead to pain in the surrounding tissues and the rejection of the implant by the host, finally resulting in implantation failure. Thus, addressing the issue of non-specific adsorption on implantable materials is a key concern in the field of biomedicine.[24,25] Nevertheless, little attention has been paid to the anti-protein adsorption ability of these implantable anisotropic hydrogels.[20,26–28] Moreover, an implantable hydrogel with the ability to convert deformation to detectable electrical signals can be very useful in artificial tendons to monitor and assess the functional recovery of joints. Recent developments of conductive hydrogels as flexible sensors for detecting various human movements in real-time have been widely reported.[29] Nevertheless, less effort has been devoted to introducing the self-sensing ability into the implantable anisotropic hydrogels for the management of artificial tendon assessment. This limitation is mainly attributed to the swelling property and non-biocompatibility of these hydrogels. To date, there has not been a report on anisotropic conductive hydrogels that is capable of simultaneously achieving the combination of high mechanical property, excellent anti-swelling behavior, and excellent biocompatibility.

Herein, we report an anisotropic, high-strength, tough, and conductive hydrogel with excellent anti-swelling ability and superior biocompatibility, demonstrating its great potential to serve as a multifunctional implantable artificial tendon. In this system, poly(vinyl alcohol) (PVA) and cellulose nanofiber (CNF) are chosen as the biocompatible polymer matrix and the collagen-mimicking nanofiber reinforcing filler, respectively, and poly (3,4-ethylenedioxythiophene):poly (styrene sulfonic acid) (PEDOT:PSS) is selected as the conducting component due to its high electrical conductivity and good hydrophilicity. Uniquely, by coupling prestretching-regulated oriented arrangement and drying-induced strengthening, a dense and stable interconnected polymer network of a hierarchically anisotropic structure is formed, with highly entangled chains crosslinked by crystalline domains and hydrogen bonding among PVA, CNF, and PEDOT:PSS. The high hydrophilicity of PVA, especially —COOH in CNF allows rapid and effective rehydration, so PCPP-D&S hydrogel with a dense network can absorb a large amount of water after soaking in deionized water. These endow the obtained anisotropic conductive hydrogel with significantly enhanced mechanical properties (tensile strength of 3.71 MPa, elastic modulus of 1.1 MPa, and toughness of 9.86 MJ m^{-3}) and a high-water content of 72.5 wt% while maintaining the excellent anti-swelling ability, a highly desirable underwater stability for implant materials. Importantly, the hydrogel also has excellent biocompatibility with remarkable protein resistance that is demonstrated in vitro and in vivo. Meanwhile, its good strain sensitivity and reliable durability enable the detection of different types of joint movement underwater. With these, this hydrogel, acting as an artificial tendon in an in vitro model, effectively restores the motion function of the joint while simultaneously monitoring the real-time motion of the joint. Finally, it is successfully implanted at the tendon defect site in a rat model and greatly promoted the restoration of animals' motion function. This work provides a valuable reference to the preparation of a new type of anisotropic hydrogel system for applications in intelligent implantable artificial tissue materials.

2. Results and Discussion

2.1. Design of Conductive Hydrogels with High Strength and Anti-Swelling Properties

In order to achieve a conductive hydrogel with excellent anti-swelling and mechanical properties, we proposed a drying and rehydration approach to promote the densification of the polymer network. The fabrication process and building blocks of the hydrogels are illustrated in **Figure 1**a. Specifically, PVA was chosen as the main matrix due to its tunable crystalline structure and good biocompatibility,[30] and CNF was selected as a nanoreinforcing filler to enhance the mechanical properties of the hydrogels owing to its superior mechanical strength, collagen-mimicking building blocks and rich hydrogen bond sites.[31,32] In addition, PEDOT:PSS was added as the conductive component due to its high conductivity, biocompatibility, and good dispersion in water.[33] The first step involved preparing the loosely crosslinked PVA/CNF/PEDOT:PSS hydrogel via freeze-thawing treatment of the precursor solution containing PVA, CNF, and PEDOT:PSS (referred to as PCPP hydrogel). During this stage, the crystalline domains between PVA chains, along with hydrogen bonding interactions between PVA, CNF, and PEDOT:PSS chains were established, but the formed network structure had a low degree of cross-linking due to the sparse entanglement between polymer chains. Subsequently, the peripheral edges of the PCPP hydrogel were fixed with clamps to induce shrinkage in the thickness direction during drying under atmospheric conditions (as the edges of the hydrogel were fixed, the hydrogel thinned significantly only in the thickness direction while did not shrink horizontally during drying.) This process facilitated the condensing of polymer chains, leading to the formation of more crystalline domains and extensive hydrogen bonding between CNF and PVA.[18] By soaking the dried PCPP film in aqueous media, the high hydrophilic nature of PVA and CNF allowed the rapid and effective rehydration, allowing the final hydrogel to have a

© 2023 Wiley-VCH GmbH

16163028, 0, Downloaded from https://onlinelibrary.wiley.com/doi/10.1002/adfm.202309500 by University of California - Los Ange, Wiley Online Library on [21/12/2023]. See the Terms and Conditions (https://onlinelibrary.wiley.com/terms-and-conditions) on Wiley Online Library for rules of use; OA articles are governed by the applicable Creative Commons License

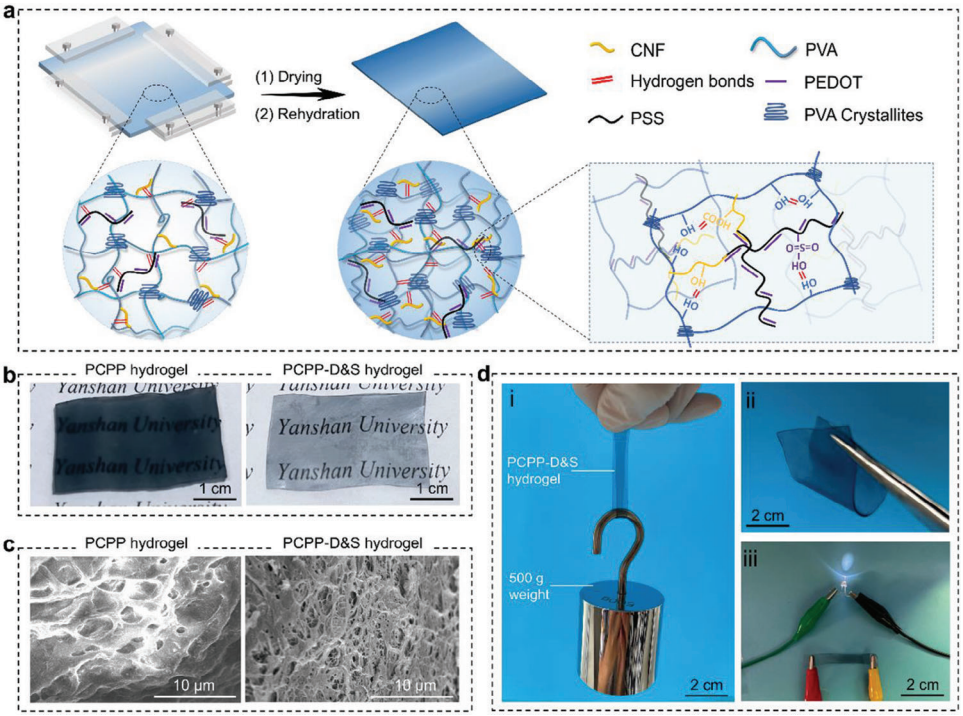

Figure 1. Schematic diagrams of fabrication and properties of the PCPP-D&S hydrogel. a) The drying-induced strengthening preparation procedure and the crosslinked structure of the PCPP-D&S hydrogel. b) Optical images and c) SEM images of the PCPP and PCPP-D&S hydrogels. d) Photographs showing i) a hydrogel strip lifting a 500 g weight, ii) a hydrogel slice being flexible for bending, and iii) a hydrogel strip lighting up the LED light.

densified network and a high equilibrium water content (referred to as PCPP-D&S hydrogel).

Photos showed that the PCPP hydrogel with 2 mm thickness exhibited low transparency. After the restrictive drying treatment and rehydration, the thickness of the resulting PCPP-D&S hydrogel was considerably reduced (≈0.4 mm) with elevated transparency (Figure 1b). This uniform shrinkage along the thickness direction led to the densification of the crosslinked structure. Structural evolution before and after the reconstruction of crosslinked structure was explored using scanning electron microscopy (SEM), as shown in Figure 1c. The pristine PCPP hydrogel had a typical porous structure with large pore sizes ranging from 1 to 6 μm, indicating the loosely crosslinked network. Remarkably, the PCPP-D&S hydrogel exhibited smaller microporous structures (0.2–2 μm) with highly interconnected compact networks and also showcased high mechanical performances. For example, the flexible PCPP-D&S hydrogel strip was strong enough to withstand a 500 g load without breakage (Figure 1di,ii). In addition, the PCPP-D&S hydrogel also exhibited good conductivity, evidenced by its ability to light up an LED light (Figure 1diii).

2.2. Mechanical Properties, Strengthening Mechanism, and Anti-Swelling Behavior of PCPP-D&S Hydrogel

The mechanical performances of the hydrogels were assessed through tensile tests. Although the addition of CNF and PEDOT:PSS contributed to the improvement of mechanical strength, the PCPP hydrogel was still mechanically weak with tensile strength of 0.45 MPa, elongation at break of 230%, elastic modulus of 0.1 MPa, and toughness of 0.5 MJ m^{-3} (**Figure 2a** and Figure S1, Supporting Information). After the reconstruction to densify the crosslinked network, PCPP-D&S hydrogel exhibited remarkably enhanced mechanical properties with a tensile strength of 2 MPa, elongation at break of 490%, elastic modulus of 0.45 MPa, and toughness of 3.74 MJ m^{-3}. It was notable that the tensile strength and toughness of the PCPP-D&S hydrogel were 4.4 and 7.4 times higher than those of the PCPP hydrogel, respectively. In this improved hydrogel, the CNF could form hydrogen bonds with PVA chains and PEDOT:PSS, playing an important role in enhancing mechanical strength.[31,32] As the CNF content increased from 0 to 2 mg mL^{-1}, the tensile strength and toughness of the PCPP-D&S hydrogel increased from 1.2 MPa and 2.21 MJ m^{-3} to 2 MPa and 3.74 MJ m^{-3}, respectively (Figure S2, Supporting Information). Further increasing CNF content to 3 mg mL^{-1} or more led to a decrease in mechanical performance, possibly due to the excess CNF disrupting the crystallization of PVA chains, which was confirmed by the X-ray diffraction (XRD) spectrum (Figure S3, Supporting Information). In addition, the mechanical properties of the PCPP-D&S hydrogel can be tuned by varying the PVA content. When the content of PVA increased from 6 to 10 wt%, the tensile mechanical performances of the PCPP-D&S hydrogel exhibited a monotonical increase (Figure S4, Supporting Information). However, high PVA content (>12 wt%) led to a slight decrease in both tensile strength and toughness. This phenomenon was related to the fact that the high crosslinking density of polymer chains at excessively high PVA concentration limited polymer motion during the stretching, resulting in premature fracture.[34] Although the

© 2023 Wiley-VCH GmbH

16163028, 0, Downloaded from https://onlinelibrary.wiley.com/doi/10.1002/adfm.202309500 by University of California - Los Angeles, Wiley Online Library on [21/12/2023]. See the Terms and Conditions (https://onlinelibrary.wiley.com/terms-and-conditions) on Wiley Online Library for rules of use; OA articles are governed by the applicable Creative Commons License

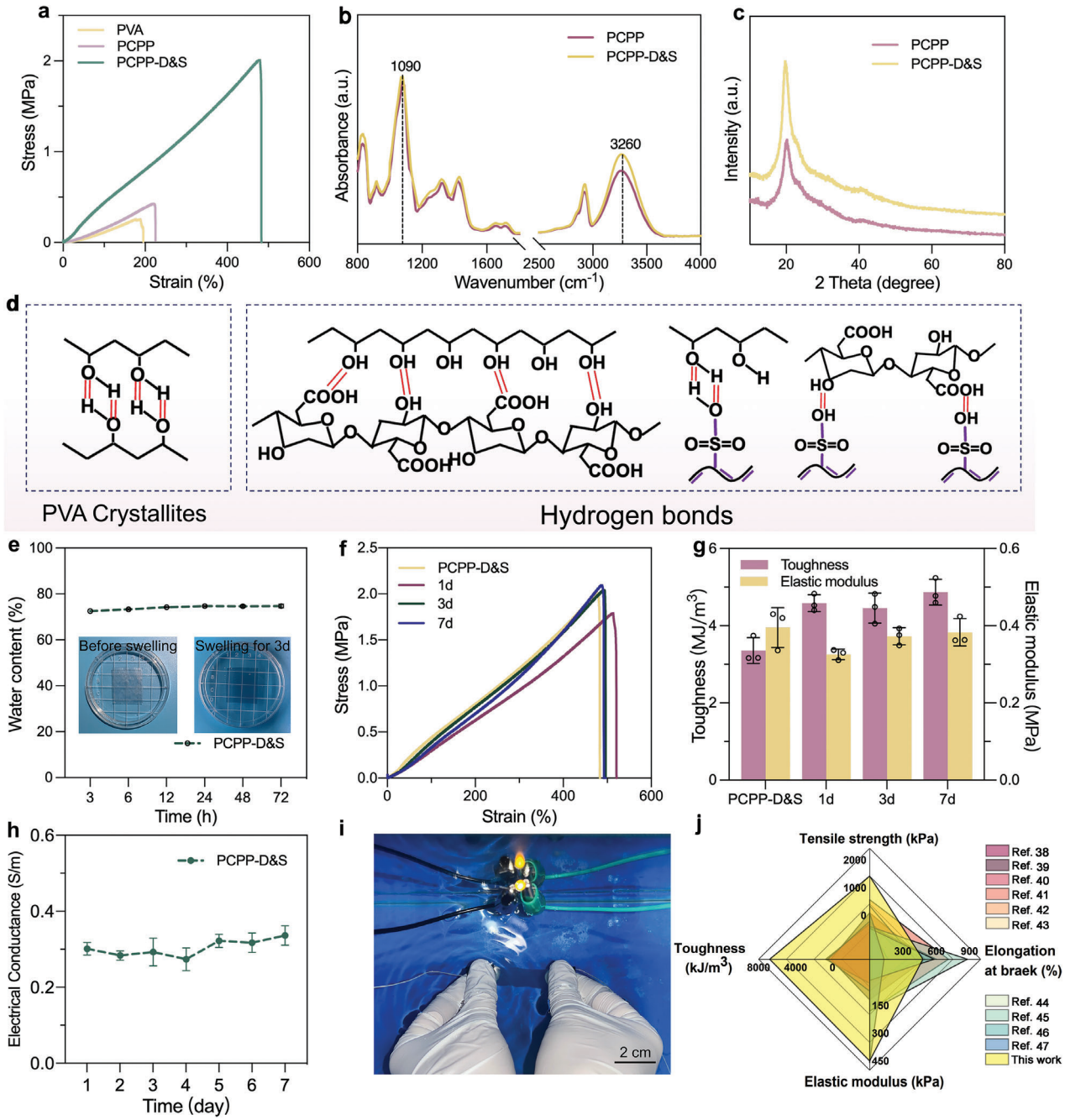

Figure 2. Mechanical, structural, and anti-swelling properties of PCPP-D&S hydrogel. a) Stress–strain curves of PVA, PCPP, and PCPP-D&S hydrogels. b) Fourier-transform infrared (FTIR) spectra and c) X-ray diffraction (XRD) of PCPP and PCPP-D&S hydrogels. d) Crosslinked structure of PCPP-D&S hydrogel. e) Water content of PCPP-D&S hydrogel in deionized water for 72 h. f) Stress–strain curves and g) elastic modulus and toughness of PCPP-D&S hydrogel in deionized water for different time periods. h) The conductivity of PCPP-D&S hydrogel in deionized water for various time periods. i) Photo showing hydrogel conductor can still light up the LED light after being immersed in deionized water for 7 days. j) A qualitative comparison between PCPP-D&S hydrogel and previously reported anti-swelling hydrogels. Error bars correspond to standard deviations.

introduction of PEDOT:PSS had a slight effect on the mechanical properties, its primary purpose was to dope and homogeneously disperse PEDOT:PSS to endow the PCPP-D&S hydrogel with suitable conductivity (Figure S5, Supporting Information).

The greatly improved high strength and superior toughness of the PCPP-D&S hydrogel originated from the increased multiple crosslinked interactions and nano-enhancement effect of CNF in the densified network. The shrinkage of the hydrogel during the drying stage caused the polymer chains to come close together.[21] Intermolecular interactions including hydrogen bonds and molecular entanglement between PVA, CNF, and PEDOT:PSS enhanced, and crystalline domains bonded by PVA

© 2023 Wiley-VCH GmbH

16163028, 0, Downloaded from https://onlinelibrary.wiley.com/doi/10.1002/adfm.202309500 by University of California - Los Ange, Wiley Online Library on [21/12/2023]. See the Terms and Conditions (https://onlinelibrary.wiley.com/terms-and-conditions) on Wiley Online Library for rules of use; OA articles are governed by the applicable Creative Commons License

chains increased. Subsequent rehydration endowed the PCPP-D&S hydrogel with high water content while maintaining the formed multiple crosslinking interactions in the densified network, thereby greatly strengthening the hydrogel. To confirm the related strengthening mechanism, a series of characterizations were conducted. Fourier transform infrared spectroscopy (FTIR) spectra (Figure S6a, Supporting Information) showed the broad peak of O—H stretching vibration at 3000 to 3600 cm^{-1}, the peak at 1664 cm^{-1} of the stretching vibration of the —COOH in CNF and the S═O stretching vibration at 1295 cm^{-1}, confirming the successful construction of PCPP and PCPP-D&S hydrogels. In addition, compared with PCPP hydrogel, the O—H stretching vibration peak (3260 cm^{-1}) was obviously sharper and the maximum peak at 1090 cm^{-1} redshifted in the PCPP-D&S hydrogel, demonstrating the increase of hydrogen bonding between polymer chains and the crystalline domains (Figure 2b and Figure S6b,c, Supporting Information).[35] The XRD spectrum (Figure 2c) revealed that the diffraction peak at 2θ = 19.7° corresponding to the (101) reflection plane of semicrystalline PVA in the PCPP-D&S hydrogel became sharper compared with that of the PCPP hydrogel, indicating the formation of more crystalline domains. This was further supported by the Raman spectra (Figure S7, Supporting Information), where the intensity of broad peaks increased significantly after the drying-induced densification.[27,36] In addition, the differential scanning calorimetry (DSC) results indicated that the freezing point and melting point of water in PCPP-D&S hydrogel were significantly lower than those in PCPP hydrogel (Figure S8, Supporting Information). This suggested that more crystalline domains nucleated during the drying process of the hydrogel, which interfered with the formation of hydrogen bonds between water molecules, thus preventing the freezing of water in the gel network.[37] These characterizations collectively confirm the structural changes in the PCPP-D&S hydrogel, which contribute to its enhanced mechanical properties.

Current high-strength hydrogels usually swell in aqueous environments, leading to a degradation of their mechanical property and functionality. This limits their applications in liquid environments such as in vivo settings. The dense hydrogen bonds and crystalline domains formed after drying and rehydration can effectively resist the attack of water molecules (Figure 2d), endowing the PCPP-D&S hydrogel with excellent anti-swelling properties. When the dried PCPP hydrogel was immersed in deionized water, it could rapidly reach swelling equilibrium within a short time (within 2 h, Figure S9, Supporting Information), resulting in the reconstructed PCPP-D&S hydrogel. The PCPP-D&S hydrogel remained stable without significant size changes (Figure 2e, inset pictures), while the size of a rectangular PCPP hydrogel showed an obvious increase after 3 days of immersion (Figure S10a, Supporting Information). The real-time swelling curves in Figure 2e show that the PCPP-D&S hydrogel achieved an almost unchanged water content of 75 wt% in deionized water for 3 days comparable to natural tendon's 60–80 wt% water content. Next, the mechanical performance of the PCPP-D&S hydrogel after swelling in deionized water within 7 days was evaluated (Figure 2f,g). With the extension of time, the mechanical properties of the PCPP-D&S hydrogel remained almost unchanged, demonstrating superb mechanical stability, while the mechanical property of the PCPP hydrogel greatly deteriorated after swelling for 7 days (Figure S10b, Supporting Information). Moreover, the conductivity of the PCPP-D&S hydrogel can also remain stable during the immersion for 7 days (Figure 2h), as demonstrated by its ability to still light up the LED light (Figure 2i). To further simulate the physiological environment, the anti-swelling property of the PCPP-D&S hydrogel in phosphate-buffered saline (PBS) solution was explored. It was observed that PCPP-D&S hydrogel immersed in PBS solution for 7 days had excellent mechanical performances and the tensile strength was even much higher than the initial state (2 vs 3 MPa, Figure S11, Supporting Information). This may be attributed to the presence of salt ions that shielded the carboxyl groups on CNF, prompting the formation of more hydrogen bonds. As a notable example, several essential parameters about the PCPP-D&S hydrogel were listed (including tensile strength, elongation at break, elastic modulus, and toughness), which were compared with recently reported anti-swelling hydrogels.[38–47] The hydrogel presented in this work possessed the best combination of anti-swelling, tensile strength, elastic modulus, and toughness, which endowed it with great potential application in the field of implantable structural materials (Figure 2j and Table S1, Supporting Information).

2.3. Prestretching-Mediated Network Structure for Constructing Anisotropic PCPP-SD&S Hydrogel with Enhanced Mechanics

To replicate the characteristics of the natural tendon such as a hierarchically anisotropic structure and high mechanical strength, a uniaxial pre-stretching was combined with the drying-rehydration process applied to isotropic PCPP hydrogel (**Figure 3a** and Figure S12, Supporting Information). When the PCPP hydrogel was uniaxially stretched, the fibrillar network was aligned in the direction of the tensile stress. In the subsequent drying process with its length fixed along the stretching direction, directionally aligned nanofibers were confined through hydrogen bonds, resulting in a permanently oriented fibrillar network.[48] After the rehydration in aqueous media, the hydrogel with anisotropic structure formed (referred to as PCPP-SD&S hydrogel). The SEM results revealed a unique tendon-like microstructure of PCPP-SD&S hydrogel (Figure 3b and Figure S13, Supporting Information), in contrast to that of the isotropic PCPP-D&S hydrogel (Figure 1c). The axial section in PCPP-SD&S hydrogel showed a highly aligned layered fiber structure with fiber diameters of 20 to 200 nm (in tendons, the cell-attached collagen fibers are in the range of 50–200 nm in diameter and 3–10 µm in length).[49,50] To further evaluate the anisotropic structure, the hydrogel was examined by polarization optical microscope (POM) with the hydrogel sample placed between the orthogonal polarizer and plane of the analyzer to observe the POM images.[18] As a control, the POM image of PCPP-D&S hydrogel was completely dark in the orthogonal direction. Even when the sample was deflected by 45° with respect to the stage, the POM image was still completely dark, indicating its isotropic structure (Figure S14, Supporting Information). In contrast, for PCPP-SD&S hydrogel, a completely dark POM image was displayed in the orthogonal direction, while a bright image appeared when the sample was deflected by 45° (Figure 3c).[20] The alternation of light and dark changes confirmed that PCPP-SD&S hydrogel was optically anisotropic, which was consistent with SEM observation.

© 2023 Wiley-VCH GmbH

16163028, 0, Downloaded from https://onlinelibrary.wiley.com/doi/10.1002/adfm.202309500 by University of California - Los Ange, Wiley Online Library on [21/12/2023]. See the Terms and Conditions (https://onlinelibrary.wiley.com/terms-and-conditions) on Wiley Online Library for rules of use; OA articles are governed by the applicable Creative Commons License

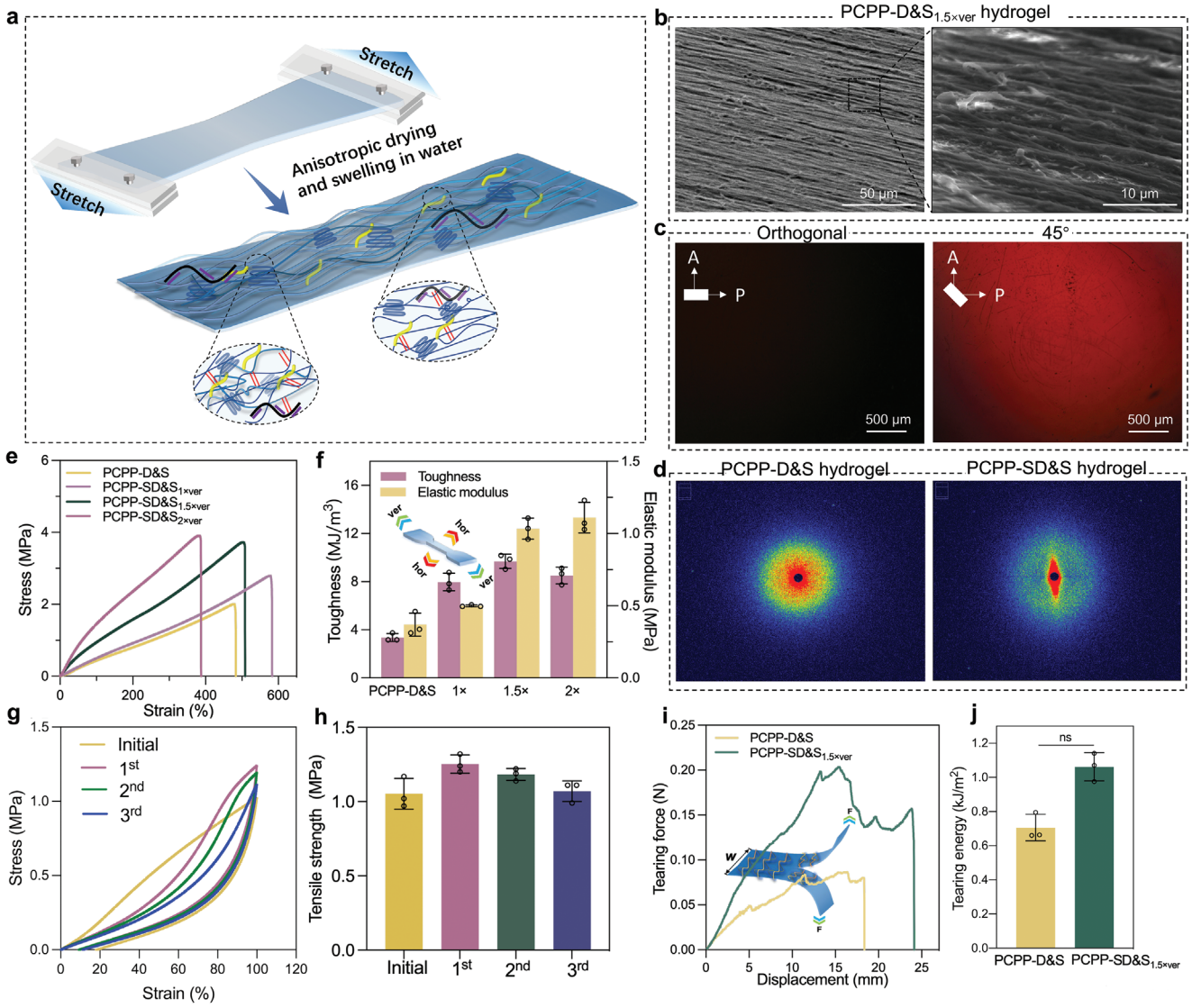

Figure 3. Construction and properties of anisotropic PCPP-SD&S hydrogel with enhanced mechanics. a) Schematic illustration of preparing the hierarchically anisotropic structure of PCPP-SD&S hydrogel. b) SEM images of PCPP-SD&S hydrogels along the pre-stretching direction (vertical). c) Polarizing optical microscopy (POM) images of PCPP-SD&S hydrogel in the orthogonal orientation and after the samples were deflected by 45°. d) SAXS patterns of PCPP-D&S and PCPP-SD&S hydrogels. Scale bar: 0.05 $Å^{-1}$. e) Stress–strain curves and f) elastic modulus and toughness of PCPP-D&S and PCPP-SD&S hydrogels obtained by controlling different degrees of uniaxial pre-stretching (100%, 150%, and 200%). Inset: ver is for vertical, along the pre-stretching direction; hor is for horizontal, perpendicular to the pre-stretching. g) Cyclic loading–unloading curves and h) tensile strength at a maximum strain of 100% after 1 h of relaxation underwater between two consecutive tests. i) Tearing curves (Inset: Schematic diagram showing the tearing process of the anisotropic PCPP-SD&S hydrogel) and j) corresponding dissipated energy of PCPP-D&S and PCPP-SD&$S_{1.5×ver}$ hydrogels. Error bars correspond to standard deviations.

From small-angle X-ray scattering (SAXS), it could be seen that the 2D pattern of PCPP-D&S showed uniform scattering rings at all different azimuths, while the PCPP-SD&S hydrogel displayed a shuttle-shaped scattering pattern (Figure 3d), further revealing the highly oriented fibrillar network of the PCPP-SD&S hydrogel.[26]

The stretching-induced formation of the oriented fiber structure greatly affected the mechanical properties of PCPP-SD&S hydrogel. The oriented fiber structure and interfibrillar interactions could be controlled by adjusting the degree of uniaxial stretching. Thus, we prepared a series of PCPP-SD&S hydrogels with 100%, 150%, and 200% prestretching strains, denoted as PCPP-SD&$S_{1×}$, PCPP-SD&$S_{1.5×}$, and PCPP-SD&$S_{2×}$, respectively. The mechanical properties of these hydrogels were then investigated. Apparently, the PCPP-SD&S hydrogel showed distinct mechanical properties in the parallel (PCPP-SD&S_{ver}) and perpendicular (PCPP-SD&S_{hor}) direction relative to the alignment direction. For example, the PCPP-SD&$S_{1.5×ver}$ hydrogel exhibited significant mechanical reinforcement in terms of strength, stiffness, and toughness, while the stretching-induced orientation resulted in a decrease in the mechanical properties of the PCPP-SD&$S_{1.5×hor}$ hydrogel (Figure S15, Supporting

© 2023 Wiley-VCH GmbH

16163028, 0, Downloaded from https://onlinelibrary.wiley.com/doi/10.1002/adfm.202309500 by University of California - Los Ange, Wiley Online Library on [21/12/2023]. See the Terms and Conditions (https://onlinelibrary.wiley.com/terms-and-conditions) on Wiley Online Library for rules of use; OA articles are governed by the applicable Creative Commons License

Information). This difference may be attributed to the different contributions from fibers oriented in different directions. As the prestretching strains increased, the tensile strength and elastic modulus of the PCPP-SD&S$_{ver}$ hydrogel gradually increased, while the tensile strain gradually decreased, and the toughness first increased and subsequently decreased (Figure 3e,f). The PCPP-SD&S$_{1.5\times ver}$ hydrogel exhibited the best combination of the high tensile strength (3.71 MPa), elastic modulus (1.1 MPa), toughness (9.86 MJ m^{-3}), and elongation at break (505%). The strength, modulus, and toughness values were 1.9, 2.4, and 2.6 times higher than those of the corresponding isotropic PCPP-D&S hydrogel. Moreover, the properties of PCPP-SD&S$_{1.5\times ver}$ hydrogel remained stable in an aqueous environment with high water content (72.5 wt%) similar to isotropic PCPP-D&S hydrogel (Figure S16, Supporting Information), indicating excellent anti-swelling property.

As load-bearing materials, the hydrogels are inevitably subjected to repeated external forces during use. The cyclic loading–unloading test was conducted to examine whether the formation of the directional fibrillar network affected the mechanical energy dissipation.[51] At the maximum strain of 200%, the PCPP-SD&S$_{1.5\times ver}$ hydrogel exhibited a more pronounced hysteresis loop with dissipation energy as high as 900 kJ m^{-3}. The higher hysteresis compared to PCPP-D&S hydrogel (Figure S17, Supporting Information) demonstrated the enhanced energy dissipation capability due to the interplay of the fibrillar network. Furthermore, the dissipation energy of PCPP-SD&S$_{1.5\times ver}$ hydrogel was significantly higher than PCPP-SD&S$_{1.5\times hor}$ hydrogel, clearly representing that PCPP-SD&S$_{1.5\times ver}$ hydrogel was not only structurally but also mechanically anisotropic. A successive cyclic tensile test on an unnotched PCPP-SD&S$_{1.5\times ver}$ sample at a maximum strain of 50% without resting time between each cycle was conducted to evaluate the fatigue hysteresis. The loading–unloading curves of the hydrogel reached steady states after only ten cycles, and the hysteresis loops were almost overlapping where the maximum nominal stress remained nearly steady in the subsequent 600 cycles (Figure S18, Supporting Information). These results proved that the hydrogel had good fatigue resistance. As illustrated in Figure 3g, more than 80% of the hysteresis can be recovered after 60 min of relaxation underwater at 100% strain for three loadings, indicating that most of the sacrificial hydrogen bonds responsible for energy dissipation can reform during the relaxation step. It is noteworthy that the maximum stress can recover to a larger value than the initial state after three loading–unloading cycles (Figure 3h). This can be attributed to some polymer chains being unzipped during the loading–unloading cycle and rearranged to form more optimized hydrogen bonds in the relaxation stage, resulting in stronger mechanical properties.[52] This self-recovery ability was of great significance and can effectively extend the service life of materials.[53] In addition, the aligned fibrous network can effectively prevent crack propagation, giving the hydrogel good fracture resistance. The energy per unit area required for the fracture of aligned nanofibers during the stretching process was higher than that of the corresponding unordered polymer chains. As a result, the tearing energy of the PCPP-SD&S$_{1.5\times ver}$ hydrogel (1.07 kJ m^{-2}) was higher than that of isotropic PCPP-D&S hydrogel (0.7 kJ m^{-2}, Figure 3i,j). Moreover, we also performed cyclic tensile tests for the notched PCPP-D&S hydrogel sample. The notched specimen was cyclically stretched 1000 times at a rate of 50 mm min^{-1}. The results showed that after 1000 times of cyclic stretching of the hydrogel sample with a large notch of 2 mm, the crack barely propagated (Figure S19 and Video S1, Supporting Information). Even when the incision samples were manually stretched with greater force, there was still no fracture (Video S2, Supporting Information). The formation of an aligned layered fiber structure facilitates the stress transfer between individual fibrils and prevents inter-fibril sliding. As a result, energy dissipation ahead of a crack tip expands to the entire network, effectively hindering the notch propagation. These results demonstrated that the hydrogel was insensitive to cracks and highly fatigue-resistance to defects and damage. In summary, the resulting hydrogel showed an anisotropic structure with an extraordinary combination of strong mechanical properties (including strength, fatigue resistance, and self-recoverability). This simple strengthening and structural orientation mechanism has great potential in constructing the anisotropic hydrogel with high mechanical performances as biomimetic artificial tissues.

2.4. Biocompatibility and Antifouling Ability of the PCPP-SD&S Hydrogel

The cytotoxicity of the PCPP-SD&S hydrogel was assessed using the Cell Counting Kit-8 (CCK-8) assay and live/dead staining of L929 fibroblasts. The fluorescent images in **Figure 4a** show that the L929 cells incubated with 50% and 100% hydrogel extracts displayed high activity (green) with good spindle morphology and only a few dead cells (red) were observed. This was similar to that of the L929 cells incubated with the RPMI 1640 medium (the control group). Figure 4b shows the result of the cell viability tested by the CCK-8. The cell viability remained above 80% after 24 and 48 h culturing in 50% and 100% hydrogel extracts compared to the control group, indicating the good cytocompatibility of the hydrogel. Foreign body reactions triggered by implanted materials can lead to surgical failure in tissue engineering and regenerative medicine. Implants in the body will be recognized and attacked by immune cells, causing immune rejection and the formation of a fibrous capsule over time, initiated by nonspecific protein adsorption onto implant surfaces followed by cell adhesion.[54] Therefore, the nonspecific protein resistance of implants is crucial to reduce the foreign body reaction. The protein resistance properties of PCPP-SD&S hydrogel were evaluated with bovine serum albumin (BSA) and fibrinogen in vitro. Compared to the tissue culture polystyrene (TCPS), the BSA and fibrinogen adsorptions of the hydrogel decreased by about 58.2% and 71.2% (Figure S20, Supporting Information, and Figure 4c). In addition, the anti-cell adhesion behavior was further assessed using L929 cells. As shown in Figure S21, Supporting Information and Figure 4d, after 12 and 24 h of incubation, a large number of L929 cells adhered to the surface of TCPS, in contrast, only a few cells adhered to the surface of the hydrogel. These results indicated that the PCPP-D&S hydrogel exhibited outstanding antifouling properties, mainly due to the superhydrophilicity of the hydrogel (Figure S22, Supporting Information) that reduced the interactions between the protein, cells, and the hydrogel through the stable hydration layer formed on the hydrogel surface.[55]

© 2023 Wiley-VCH GmbH

16163028, 0, Downloaded from https://onlinelibrary.wiley.com/doi/10.1002/adfm.202309500 by University of California - Los Ange, Wiley Online Library on [21/12/2023]. See the Terms and Conditions (https://onlinelibrary.wiley.com/terms-and-conditions) on Wiley Online Library for rules of use; OA articles are governed by the applicable Creative Commons License

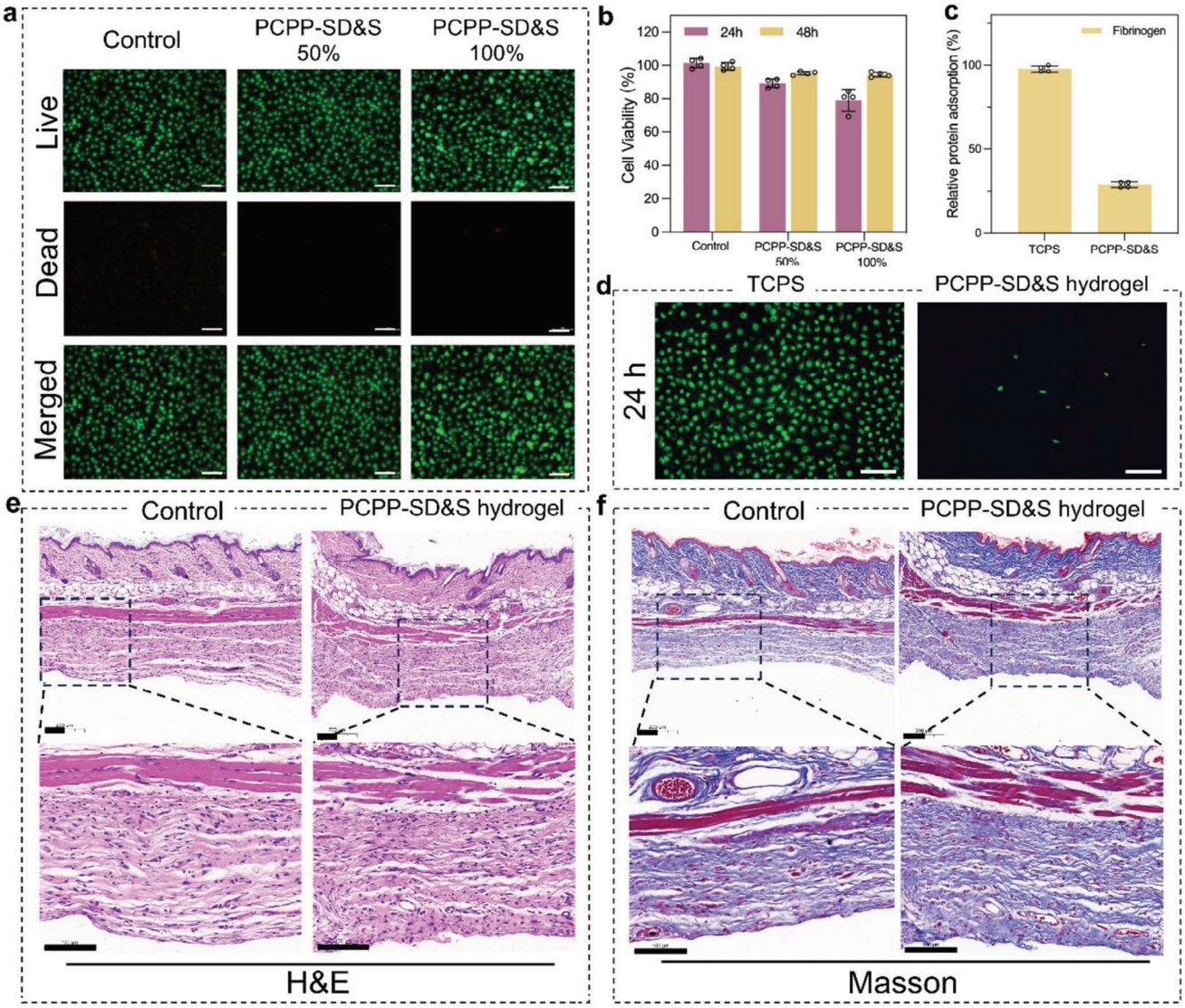

Figure 4. Anti-fouling performance and biocompatibility of the PCPP-SD&S hydrogel. a) Live/dead staining of L929 cells after 48 h of incubation with the PCPP-SD&S hydrogel extractions. Scale bars: 50 μm. b) CCK-8 assay of L929 fibroblast cells cultured in media treated with different hydrogel extracts for 24 and 48 h. c) Relative protein adsorption of fibrinogen on TCPS and the PCPP-SD&S hydrogel. d) Fluorescence images of L929 adhered onto TCPS and PCPP-SD&S hydrogel surfaces after 24 h of incubation. Scale bars: 100 μm. e) H&E and f) Masson's trichrome staining of tissue sections surrounding the implants after 2 weeks. Scale bar: 200 μm. Error bars correspond to standard deviations.

To further assess the suitability for in vivo biomedical applications, the PCPP-SD&S hydrogel was implanted subcutaneously on the back of mice for 1 and 2 weeks, respectively. Skin tissues in contact with the hydrogel sample were collected from mice after 1 and 2 weeks, and skin tissues collected from mice that did not undergo any surgeries were selected as the negative control. All skin tissues were treated with hematoxylin-eosin (H&E) and Masson's trichrome staining for further histological analysis. As shown in the H&E staining images in Figure S23a, Supporting Information, after 1 week of implantation, a few inflammatory cell aggregations were observed at the interface between the tissue and the implanted hydrogel, compared to the negative control. After increasing the post-surgery observation time to 2 weeks, very few inflammations were observed, which was similar to the negative control (Figure 4e). These results indicated that few inflammations were observed after 1 week of the hydrogel implantation, and the inflammatory reaction was alleviated after 2 weeks. Furthermore, Masson's trichrome staining was then applied to observe the formation of a fibrous capsule around the hydrogel. After 1 week of operation, the interface between the tissue and the implanted hydrogel showed a slightly thicker fibrous capsule than that of the control group (Figure S23b, Supporting Information). After 2 weeks of operation, no obvious fibrous capsule formation was observed, which was similar to the healthy tissue in the negative control (Figure 4f). Overall, these results showed that the PCPP-SD&S hydrogel demonstrated excellent biocompatibility both in vitro and in vivo, without causing obvious inflammatory response and foreign body reaction.

© 2023 Wiley-VCH GmbH

16163028, 0, Downloaded from https://onlinelibrary.wiley.com/doi/10.1002/adfm.202309500 by University of California - Los Ange, Wiley Online Library on [21/12/2023]. See the Terms and Conditions (https://onlinelibrary.wiley.com/terms-and-conditions) on Wiley Online Library for rules of use; OA articles are governed by the applicable Creative Commons License

2.5. Demonstration of the Potential Application as Intelligent Artificial Tendon

Typically, when artificial materials are used as the substitute for an injured tendon, there is an absence of effective monitoring of the injury recovery process. The continuous monitoring of joint motion during the restoration process is significant for joint motion rehabilitation. Empowering artificial materials with sensing properties can quantitatively and continuously monitor and evaluate the rehabilitation of joint motion. The PCPP-SD&S hydrogel has good conductivity (0.3 S m^{-1}) and thus can serve as a sensor to monitor mechanical deformation. First, we evaluated the strain-sensing performances of the hydrogel (Figure S24, Supporting Information). Strain factor (gauge factor, GF) is an important parameter to evaluate the sensitivity of a sensor, defined as $GF = (\Delta R/R_0)/\epsilon$, where ΔR is resistance variation, R_0 is the initial resistance, and ϵ is tensile strain.[56] The GFs were 0.88 and 1.30 in the strain regions of 0–50% and 50-505%, respectively, exhibiting the two-staged linear response with high sensitivity (Figure S24a, Supporting Information). The response signals at different cyclic strains (10%, 30%, and 50%) greatly varied and the patterns of each cycle were highly similar at the same strain (Figure S24b, Supporting Information), indicating the hydrogel could differentiate different levels of strains with superior reliability. The peak variations of the relative resistance are almost the same at different stretching rates and the $\Delta R/R_0$ signals were nearly reproducible at a strain of 50% over 600 cycles (Figure S24c,d, Supporting Information). These results validate that the hydrogel had good dynamic stability and long-term reliable sensing performances. The overall sensing performance and excellent anti-swelling property enabled the PCPP-SD&S hydrogel sensor to find potential applications in monitoring joint motion in a wet environment. When such strain-sensing hydrogels were fixed on human joints (fingers, elbows, and knees), a stable repetitive response was observed as the joint bent with different motion amplitudes underwater (Figure S25, Supporting Information). The hydrogel sensor can respond to the target motion in time and output the sensing signal in real-time, presenting its potential as a smart artificial tendon capable of real-time joint motion monitoring.

The tendon-mimicking anisotropic structure, high mechanical strength, excellent anti-swelling property, good biocompatibility, and outstanding underwater self-sensing capability all point to the PCPP-SD&S hydrogel being a good candidate for intelligent artificial tendon implants, as illustrated in **Figure** 5a,b. We first installed the hydrogel on a human knee joint model to simulate the actual application. Specifically, the tibial collateral ligament on the knee joint model was replaced by a PCPP-SD&S hydrogel. After the integration of the hydrogel into the joint site, various bending states of the joint into different angles were achieved even in fluid conditions (Figure 5a and Video S3, Supporting Information), indicating its potential of effectively restoring joint mobility as an artificial substitute of natural tendons. In the meantime, these joint bending states were monitored in real-time by the $\Delta R/R_0$ of the succedaneous hydrogel. Specifically, the observed $\Delta R/R_0$ exhibited a stepwise growth/decrease pattern when the angles were increased/decreased between 0° and 120° (Figure 5c). The $\Delta R/R_0$ value remained constant when the joint model bent to the same angle. The bending process of the joint model can be repeated and the corresponding $\Delta R/R_0$ remained basically unchanged in 100 consecutive bending cycles (Figure 5d), demonstrating the excellent durability of the hydrogel as the intelligent artificial tendon. Overall, the above in vitro experiments prove that the PCPP-SD&S hydrogel, as an artificial tendon, can not only effectively restore joint movement, but also monitor the real-time situation of joint rehabilitation.

In order to further evaluate the potential of the anti-swelling PCPP-SD&S anisotropic hydrogel for reconstructing tendon defects in clinical applications, in vivo evaluation using typical rat tendon replacement models was performed. The establishment of the rat tendon substitution model is illustrated in Figure 5e. First, the tendons of SD rats were notched in the middle using scissors. Then, the sterilized hydrogel splines were implanted into the tendon defect and fixed by suturing. After the wound was sutured, penicillin was injected regularly. For comparison, in the control group, only a notch was produced in the tendon, and penicillin was injected after the wound was sutured. It is shown in Figure 5f that the wound of the rat in the experimental group was red and swollen after 1 day of operation. After 1 week of operation, it was observed that the shape of the hind legs of the rat had basically recovered (the stitches of the experimental group had been removed), and both the redness and swelling had mostly disappeared. In contrast, in the control group, the degree of wound healing in tendon defects was significantly lower. After 2 weeks of the implantation, the exercise routine on a balance bar for the rat implanted with the hydrogel grafts essentially returned to a normal state, and the rat's balancing motion was visually observed to be better than those of the control groups (Videos S4 and S5, Supporting Information). These results demonstrate that the PCPP-SD&S hydrogel, as the tendon substitution, can effectively facilitate the restoration of the joint movement ability of the rats with injured tendons.

3. Conclusion

In summary, we have successfully developed an anisotropic conductive hydrogel with high strength, high toughness, superior swelling resistance, excellent strain sensitivity, and biocompatibility by integrating the drying-induced strengthening mechanism and pre-stretching-regulated ordered arrangement strategy. The densification of polymer chains induced by drying and rehydration led to the formation of a compact and stable network with multiple crosslinking interactions including crystalline domains and hydrogen bonds among PVA, CNF, and PEDOT:PSS chains. These interactions greatly improved the mechanical properties and anti-swelling ability of the obtained PCPP-D&S hydrogel. The integration of the uniaxial pre-stretching and drying-rehydration process resulted in a dense and permanently oriented fibrillar network confined via hydrogen bonds, which endowed the resulting hydrogel with anisotropic structure, exceptional mechanical properties, and excellent stability underwater. Moreover, the hydrogel demonstrated excellent protein-resistance and biocompatibility, without inducing any significant inflammation response or fibrous capsule formation, making it a safe option for implantable materials. In addition, the good strain sensitivity enables this anisotropic hydrogel to capture sensing signals of various joint movements underwater. As an artificial tendon in an in vitro model, the hydrogel

© 2023 Wiley-VCH GmbH

16163028, 0, Downloaded from https://onlinelibrary.wiley.com/doi/10.1002/adfm.202309500 by University of California - Los Ange, Wiley Online Library on [21/12/2023]. See the Terms and Conditions (https://onlinelibrary.wiley.com/terms-and-conditions) on Wiley Online Library for rules of use; OA articles are governed by the applicable Creative Commons License

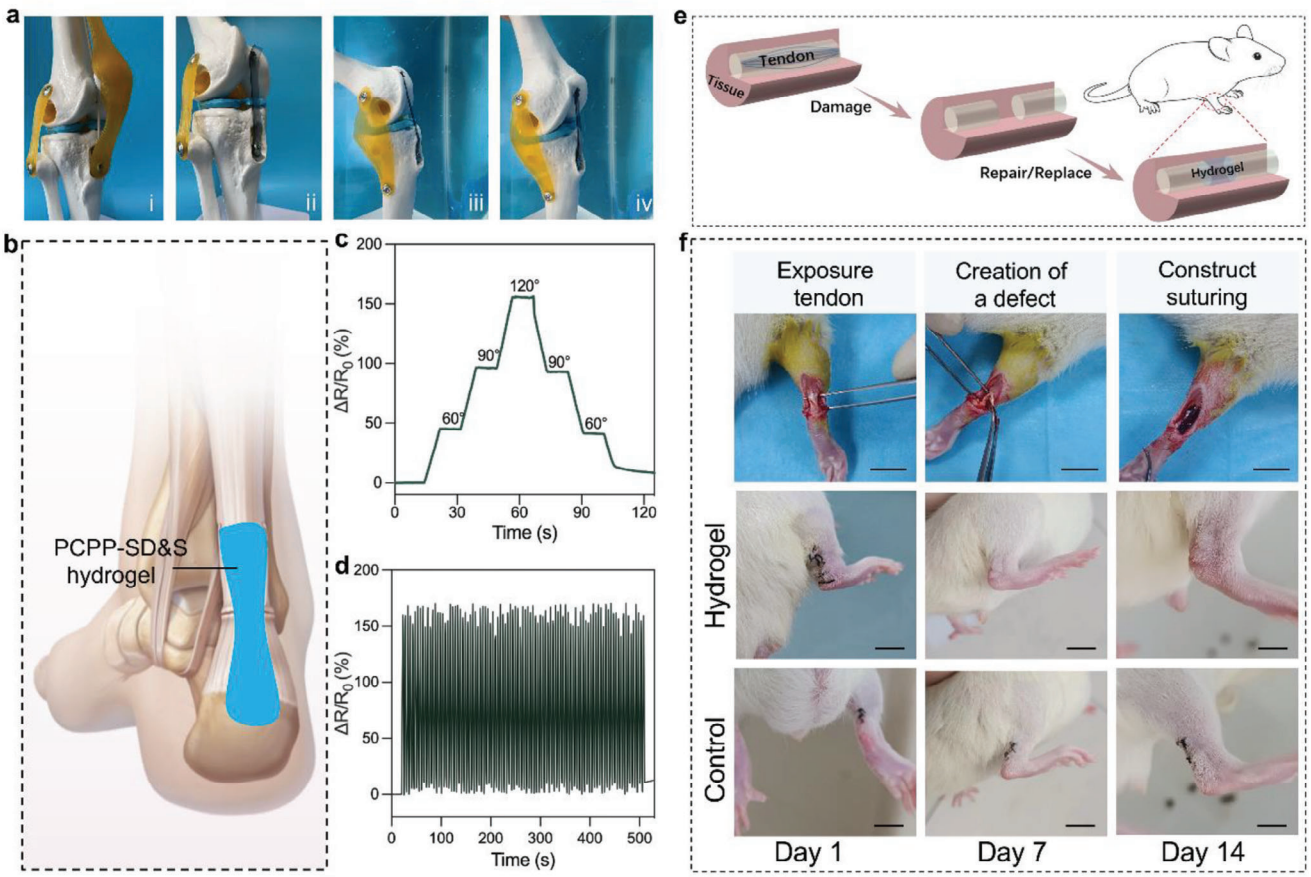

Figure 5. Potential application of the PCPP-SD&S hydrogel as intelligent artificial tendon. a) Photos of the assembled intelligent artificial tendon at different bending states: i) the original knee joint model, ii) the knee model with a PCPP-SD&S hydrogel strip attached as an artificial tendon, iii) bending at 90° underwater, and iv) returning to the vertical state. b) Schematic diagram of Achilles tendon repair with hydrogel substitute. c) Relative resistance changes ($\Delta R/R_0$) of the PCPP-SD&S hydrogel artificial tendon during the bending of tendon substitution model at various angles underwater. d) $\Delta R/R_0$ of the PCPP-SD&S hydrogel artificial tendon during tendon substitution model bending from 0° to 120° for 100 cycles. e) Schematic diagram showing the in vivo animal test process. f) The right hind limb of SD rats recovered at different times after operation with the hydrogel artificial tendon, in comparison with the rat without using the hydrogel (control). Scale bar: 1 cm.

effectively restored joint movement while monitoring the status of the joint rehabilitation. In addition, in a rat model of tendon defect, the PCPP-SD&S hydrogel showed promising performance as a tendon substitute, with animals recovering their normal motor function after a 2-week implantation period. Overall, such hydrogels hold great potential applications in therapeutics and rehabilitation, as intelligent implantable materials for treating various malfunctional tissues with stimulation and detection abilities.

4. Experimental Section

Materials: PVA (MW = 145 000; 99% hydrolyzed,) was purchased from Shanghai Aladdin Co., Ltd. CNFs (diameter: ≈10–20 nm, length: 1–2 µm, 1 wt%) were purchased from Tianjin Mujingling Technology Co., Ltd. PEDOT:PSS dispersion (Clevios PH1000, Heracus) and PBS (pH = 7.4) were purchased from Sigma-Aldrich. Fibrinogen from human plasma (≥85% of protein is clottable) was purchased from Beijing Lanjieke Technology Co. Ltd. Bicin-choninic acid (BCA) Protein Assay kit was purchased from Shanghai Beyotime Biotechnology Co., Ltd. CCK-8 and acridine orangepropidium iodide (AO/PI) Double Staining Kit were purchased from Beijing Solarbio Technology Co., Ltd. Standard fibroblast cell line L929 fibroblasts were provided by the Cell Bank of the Chinese Academy of Sciences, Shanghai, China. All solvents and chemicals were purchased from commercial sources and used without further purification unless otherwise indicated.

Synthesis of PCPP, PCPP-D&S, and Anisotropic PCPP-SD&S Hydrogels: Typically, a certain amount of PVA powders were dissolved in 10 mL deionized water and stirred for 2 h at 95 °C to form a PVA solution. Subsequently, CNF dispersions and PEDOT:PSS dispersion were added into the PVA solution under stirring for 2 h to obtain the PCPP precursor solution. After three freezing-thawing cycles, the PCPP hydrogel was prepared.

The peripheral edges of the prepared PCPP hydrogel were fixed, which was placed at 60 °C for 3 h until it was completely dried. The obtained xerogel was then immersed in deionized water for 3 days at room temperature to reach swelling equilibrium, forming isotropic drying-induced enhanced hydrogel, which was denoted as PCPP-D&S hydrogel.

The obtained PCPP hydrogel was uniaxially pre-stretched to a particular strain (100%, 150%, 200%), and the two ends of the stretched hydrogel were fixed on the mold. Then, the sample was thoroughly dried at 60 °C for 3 h (maintained in the pre-stretched condition during this process). Finally, the dried sample was immersed in water for 3 days to reach swelling equilibrium to fabricate the anisotropic PCPP-SD&S hydrogel.

© 2023 Wiley-VCH GmbH

16163028, 0, Downloaded from https://onlinelibrary.wiley.com/doi/10.1002/adfm.202309500 by University of California - Los Ange, Wiley Online Library on [21/12/2023]. See the Terms and Conditions (https://onlinelibrary.wiley.com/terms-and-conditions) on Wiley Online Library for rules of use; OA articles are governed by the applicable Creative Commons License

Characterization: The chemical structure of the hydrogel samples was characterized by FTIR spectroscopy (Thermo Nicolet Corporation) in the range of 400–4000 cm^{-1} at room temperature and Raman spectrometer (Horiba Jobin Yvon Xplora PLUS). XRD measurement was obtained by X-ray diffractometer (Rigaku, SMART LAB) under Cu-Kα radiation (λ = 1.5418 Å). DSC analysis was performed using a Discovery DSC 250 instrument under a nitrogen atmosphere. The hydrogel samples were first cooled from room temperature to −60 °C and then heated to 50 °C at a rate of 3 °C min^{-1}. The morphology and microstructure of the hydrogels were observed by an SEM (SUPRA 55, Zeiss, Germany) and POM (Nikon, LV100POL). SAXS measurements were carried out at Xeuss 2.0 (Xenocs, France) with an X-ray wavelength of 1.54 Å. The sample-to-detector distance was 1185 mm. The water contact angle (WCA) was observed by an automatic tilting contact angle measuring instrument (SDC-350, Dongguan Shengding Precision Instrument Co., Ltd.).

Statistical Analysis: Data represent the mean ± SD of at least three replicates. Statistical analyses were performed with GraphPad Prism software.

Supporting Information

Supporting Information is available from the Wiley Online Library or from the author.

Acknowledgements

The authors greatly appreciate the financial support of the National Natural Science Foundation of China (Nos. 22102139, 22072127), the Hebei Natural Science Foundation (Nos. B2021203001, B2021203016), the Science and Technology Project of Hebei Education Department (No. ZD2022147), and the Special Project for Local Science and Technology Development Guided by the Central Government of China (Nos. 216Z1301G, 226Z1401G).

Conflict of Interest

The authors declare no conflict of interest.

Data Availability Statement

The data that support the findings of this study are available from the corresponding author upon reasonable request.

Keywords

anisotropic hydrogel, anti-protein adsorption, anti-swelling, high mechanical strength, implantable electronic tendons

Received: August 11, 2023
Revised: November 5, 2023
Published online:

[1] S. F. Tellado, E. R. Balmayor, M. Van Griensven, *Adv. Drug Delivery Rev.* **2015**, *94*, 126.
[2] J. G. Snedeker, J. Foolen, *Acta Biomater.* **2017**, *63*, 18.
[3] D. Docheva, S. A. Müller, M. Majewski, C. H. Evans, *Adv. Drug Delivery Rev.* **2015**, *84*, 222.
[4] M. Benjamin, E. Kaiser, S. Milz, *J. Anat.* **2008**, *212*, 211.
[5] J. Kohler, C. Popov, B. Klotz, P. Alberton, W. C. Prall, F. Haasters, S. Müller-Deubert, R. Ebert, L. Klein-Hitpass, F. Jakob, M. Schieker, D. Docheva, *Aging Cell* **2013**, *12*, 988.
[6] J. E. Ackerman, I. Bah, J. H. Jonason, M. R. Buckley, A. E. Loiselle, *J. Orthop. Res.* **2017**, *35*, 2716.
[7] J. L. Drury, D. J. Mooney, *Biomaterials* **2003**, *24*, 4337.
[8] F. Gao, Z. Xu, Q. Liang, H. Li, L. Peng, M. Wu, X. Zhao, X. Cui, C. Ruan, W. Liu, *Adv. Sci.* **2019**, *6*, 1900867.
[9] M. Hua, S. Wu, Y. Ma, Y. Zhao, Z. Chen, I. Frenkel, J. Strzalka, H. Zhou, X. Zhu, X. He, *Nature* **2021**, *590*, 594.
[10] X. Dong, X. Guo, Q. Liu, Y. Zhao, H. Qi, W. Zhai, *Adv. Funct. Mater.* **2022**, *32*, 2203610.
[11] Y. Feng, H. Liu, W. Zhu, L. Guan, X. Yang, A. V. Zvyagin, Y. Zhao, C. Shen, B. Yang, Q. Lin, *Adv. Funct. Mater.* **2021**, *31*, 2105264.
[12] X. Guo, X. Dong, G. Zou, H. Gao, W. Zhai, *Sci. Adv.* **2023**, *9*, eadf7075.
[13] C. Luo, M. Huang, X. Sun, N. Wei, H. Shi, H. Li, M. Lin, J. Sun, *ACS Appl. Mater. Interfaces* **2022**, *14*, 2638.
[14] M. Sun, H. Li, Y. Hou, N. Huang, X. Xia, H. Zhu, Q. Xu, Y. Lin, L. Xu, *Sci. Adv.* **2023**, *9*, eade6973.
[15] D. Ji, T. L. Nguyen, J. Kim, *Adv. Funct. Mater.* **2021**, *31*, 2101095.
[16] L. Geng, W. Liu, B. Fan, J. Wu, S. Shi, A. Huang, J. Hu, X. Peng, *Chem. Eng. J.* **2023**, *462*, 142226.
[17] J. Sun, L. Xiao, B. Li, K. Zhao, Z. Wang, Y. Zhou, C. Ma, J. Li, H. Zhang, A. Herrmann, K. Liu, *Angew. Chem., Int. Ed.* **2021**, *60*, 23687.
[18] M. T. I. Mredha, Y. Z. Guo, T. Nonoyama, T. Nakajima, T. Kurokawa, J. P. Gong, *Adv. Mater.* **2018**, *30*, 1704937.
[19] B. Guo, S. He, M. Yao, Z. Tan, X. Li, M. Liu, C. Yu, L. Liang, Z. Zhao, Z. Guo, M. Shi, Y. Wei, H. Zhang, F. Yao, J. Li, *Chem. Eng. J.* **2023**, *461*, 142099.
[20] N. Park, J. Kim, *ACS Appl. Mater Interfaces* **2022**, *14*, 4479.
[21] D. Liu, Y. Cao, P. Jiang, Y. Wang, Y. Lu, Z. Ji, X. Wang, W. Liu, *Small* **2023**, *19*, 2206819.
[22] M. S. Draz, M. Moazeni, M. Venkataramani, H. Lakshminarayanan, E. Saygili, N. K. Lakshminaraasimulu, K. M. Kochehbyoki, M. K. Kanakasabapathy, S. Shabahang, A. Vasan, M. A. Bijarchi, A. Memic, H. Shafiee, *Adv. Funct. Mater.* **2018**, *28*, 17071.
[23] J. Olsson, V. Novy, F. Nielsen, O. Wallberg, M. Galbe, *Biotechnol. Biofuels* **2019**, *12*, 1.
[24] J. H. Werner, J. H. Rosenberg, K. L. Keeley, D. K. Agrawal, *Expert Rev. Clin. Immunol.* **2018**, *14*, 695.
[25] G. Jell, D. Kerjaschki, P. Revell, N. Al-Saffar, *J. Biomed. Mater. Res.* **2006**, *77*, 119.
[26] X. Liang, G. Chen, S. Lin, J. Zhang, L. Wang, P. Zhang, Z. Wang, Z. Wang, Y. Lan, Q. Ge, J. Liu, *Adv. Mater.* **2021**, *33*, 2102011.
[27] S. Han, Q. Wu, J. Zhu, J. Zhang, A. Chen, S. Su, J. Liu, J. Huang, X. Yang, L. Guan, *Mater. Horiz.* **2023**, *10*, 1012.
[28] S. Choi, Y. Choi, J. Kim, *Adv. Funct. Mater.* **2019**, *29*, 1904342.
[29] Z. Qin, S. Liu, J. Bai, J. Yin, N. Li, T. Jiao, *Int. J. Biol. Macromol.* **2022**, *220*, 90.
[30] S. Wu, M. Hua, Y. Alsaid, Y. Du, Y. Ma, Y. Zhao, C.-Y. Lo, C. Wang, D. Wu, B. Yao, J. Strzalka, H. Zhou, X. Zhu, X. He, *Adv. Mater.* **2021**, *33*, 2007829.
[31] F. Wang, H. Du, Y. Liu, H. Huang, X. Yu, X. Zhu, L. Li, *Synth. Met.* **2021**, *282*, 116952.
[32] J. Wei, Y. Chen, H. Liu, C. Du, H. Yu, J. Ru, Z. Zhou, *J. Energy Chem.* **2022**, *67*, 432.
[33] Q. Liu, J. Qiu, C. Yang, L. Zang, G. Zhang, E. Sakai, *Adv. Mater. Technol.* **2021**, *6*, 2000919.
[34] L. Wang, X. Zhang, Y. Xia, X. Zhao, Z. Xue, K. Sui, X. Dong, D. Wang, *Adv. Mater.* **2019**, *31*, 1902381.
[35] Y. Wu, Y. Zhang, H. Wu, J. Wen, S. Zhang, W. Xing, H. Zhang, H. Xue, J. Gao, Y. Mai, *Adv. Mater.* **2023**, *35*, 2210624.

© 2023 Wiley-VCH GmbH

16163028, 0, Downloaded from https://onlinelibrary.wiley.com/doi/10.1002/adfm.202309500 by University of California - Los Angeles, Wiley Online Library on [21/12/2023]. See the Terms and Conditions (https://onlinelibrary.wiley.com/terms-and-conditions) on Wiley Online Library for rules of use; OA articles are governed by the applicable Creative Commons License

[36] Y.-F. Zhang, M.-M. Guo, Y. Zhang, C. Y. Tang, C. Jiang, Y. Dong, W.-C. Law, F.-P. Du, *Polym. Test.* **2020**, *81*, 106213.
[37] D. Ji, J. M. Park, M. S. Oh, T. L. Nguyen, H. Shin, J. S. Kim, D. Kim, H. S. Park, J. Kim, *Nat. Commun.* **2022**, *13*, 3019.
[38] C. Hu, Y. Zhang, X. Wang, L. Xing, L. Shi, R. Ran, *ACS Appl. Mater. Interfaces* **2018**, *10*, 44000.
[39] Y. Gao, Y. Wang, Y. Dai, Q. Wang, P. Xiang, Y. Li, G. Gao, *Eur. Polym. J.* **2022**, *164*, 110981.
[40] J. Ren, Y. Liu, Z. Wang, S. Chen, Y. Ma, H. Wei, S. Lü, *Adv. Funct. Mater.* **2022**, *32*, 2107404.
[41] L. Xu, S. Gao, Q. Guo, C. Wang, Y. Qiao, D. Qiu, *Adv. Mater.* **2020**, *32*, 2004579.
[42] W. Liang, W. He, R. Huang, Y. Tang, S. Li, B. Zheng, Y. Lin, Y. Lu, H. Wang, D. Wu, *Adv. Mater.* **2022**, *34*, 2108992.
[43] H. Lu, B. Wu, X. Le, W. Lu, Q. Yang, Q. Liu, J. Zhang, T. Chen, *Adv. Funct. Mater.* **2022**, *32*, 2206912.
[44] H. Feng, J. Zhang, W. Yang, Y. Ma, R. Wang, S. Ma, M. Cai, B. Yu, F. Zhou, *ACS Appl. Mater. Interfaces* **2021**, *13*, 50505.
[45] H. Fan, J. Wang, Z. Jin, *Macromolecules* **2018**, *51*, 1696.
[46] J. Wei, Y. Zheng, T. Chen, *Mater. Horiz.* **2021**, *8*, 2761.
[47] S. Wang, D. Zhang, X. He, J. Zhou, Y. Zhou, X. Wang, Z. Wang, S. Liu, S. Y. Zheng, J. Yang, *ACS Appl. Polym. Mater.* **2022**, *4*, 7498.
[48] X. Lin, X. Xing, S. Li, X. Wu, Q. Jia, H. Tu, H. Bian, A. Lu, L. Zhang, H. Yang, B. Duan, *Adv. Funct. Mater.* **2022**, *32*, 2112685.
[49] G. Nourissat, F. Berenbaum, D. Duprez, *Nat. Rev. Rheumatol.* **2015**, *11*, 223.
[50] L. Xu, X. Zhao, C. Xu, N. A. Kotov, *Adv. Mater.* **2018**, *30*, 1703343.
[51] X. Chen, R. Li, S. H. D. Wong, K. Wei, M. Cui, H. Chen, Y. Jiang, B. Yang, P. Zhao, J. Xu, H. Chen, C. Yin, S. Lin, W. Y.-W. Lee, Y. Jing, Z. Li, Z. Yang, J. Xia, G. Chen, G. Li, L. Bian, *Nat. Commun.* **2019**, *10*, 2705.
[52] S. Lin, J. Liu, X. Liu, X. Zhao, *Proc. Natl. Acad. Sci. U. S. A.* **2019**, *116*, 10244.
[53] M. T. I. Mredha, V. T. Tran, S.-G. Jeong, J.-K. Seon, I. Jeon, *Soft Matter* **2018**, *14*, 7706.
[54] W. Lin, J. Zhang, Z. Wang, S. Chen, *Acta Biomater.* **2011**, *7*, 2053.
[55] M. Yao, Z. Wei, J. Li, Z. Guo, Z. Yan, X. Sun, Q. Yu, X. Wu, C. Yu, F. Yao, S. Feng, H. Zhang, J. Li, *Nat. Commun.* **2022**, *13*, 5339.
[56] S. Bai, S. Zhang, W. Zhou, D. Ma, Y. Ma, P. Joshi, A. Hu, *Nano-Micro Lett.* **2017**, *9*, 42.

© 2023 Wiley-VCH GmbH

16163028, 0, Downloaded from https://onlinelibrary.wiley.com/doi/10.1002/adfm.202309500 by University of California - Los Ange, Wiley Online Library on [21/12/2023]. See the Terms and Conditions (https://onlinelibrary.wiley.com/terms-and-conditions) on Wiley Online Library for rules of use; OA articles are governed by the applicable Creative Commons License